JOURNAL OF AIRCRAFT
Vol. 29, No. 5, Sept.-Oct. 1992

Euler/Experiment Correlation of a Generic Fighter

Aga M. Goodsell*
NASA Ames Research Center, Moffett Field, California 94035

Flowfields about a generic fighter model have been computed using FLO57, a three-dimensional, finite-volume Euler code. Computed pressure coefficients, forces, and moments at three Mach numbers—0.8, 1.2, and 1.6—are compared with wind-tunnel data over a wide range of angles of attack in order to determine the applicability of the code for the analysis of fighter configurations. Two configurations were studied, a wing/body and a wing/body/chine. FLO57 predicted pressure distributions, forces, and moments well at low angles of attack, at which the flow was fully attached. The FLO57 predictions were also accurate for some test conditions once the leading-edge vortex became well established. At the transonic speed, FLO57 appeared to predict vortex breakdown earlier than that seen in the experimental results. Placing the chine on the forebody delayed the onset of bursting and improved the correlation between numerical and experimental data at the subsonic conditions.

Introduction

A LARGE amount of work has been done at subsonic and supersonic speeds to provide a good understanding of the mechanisms involved in the formation and effects of the leading-edge vortices on delta wings. In a subsonic freestream condition, the flow undergoes a strong expansion at the leading edge from the windward to the leeward side. For sharp leading edges, the flow separates at the leading edge producing a free-shear layer of distributed vorticity. The separation point is fixed at the sharp leading edge for all angles of attack above that for initial separation and is independent of leading-edge geometry.[1] These leeward vortices, which occur in counter-rotating pairs as the flow is shed from opposite leading edges, are the dominant features of the flow. The vortices induce very low pressure levels on the wing surface directly below the vortex core. The resultant normal force is then much larger than that which would occur if the flow were to remain attached and the vortices were not present.[1] Secondary and tertiary vortices may form on the leeward surface of the wing if the flow in the boundary layer cannot overcome the adverse pressure gradient that exists under the primary vortex core. At supersonic speeds, experiments have shown that on highly swept wings with subsonic leading edges, the upper surface flow is similar to that at low speeds. As the Mach number increases or the sweep angle decreases, the vortices become flatter and eventually disappear, giving way to attached flow at the leading edge.[2] Further descriptions of the underlying physical phenomena for these vortical flows are contained in the works of Stanbrook and Squire[3] and Miller and Wood.[4] The physical complexity of the flowfield at transonic speeds is not well understood because of the existence of shock waves, vortex-shock interactions, vortex breakdown, and shock-boundary-layer interaction.

The objective of this article is to evaluate the solutions of transonic and low supersonic flowfields about a generic fighter with delta wings obtained from an Euler code in order to determine their validity over a wide range of angles of attack. The Navier-Stokes equations correctly model the relevant flow physics and provide a uniformly valid description of vortical flow about arbitrary geometries throughout the range of flight speeds and Reynolds numbers. However, numerical simulations of these equations require more memory and CPU time. The Euler equations provide the correct Rankine-Hugoniot shock jump conditions, the correct jump conditions for a vortex sheet, and allow for the transport of vorticity but cannot model the viscous effects present in the flowfield.

Experimental Work

In an effort to increase the understanding of vortex flows at transonic speeds, Erickson and Rogers[2] and Erickson and Schreiner[5] conducted a series of experimental investigations into the behavior of the generic fighter model at transonic conditions. The model had a 55-deg swept cropped delta wing of aspect ratio 1.8 and taper ratio 0.2. The airfoils used in the wing were modified NACA 65A005 sections with sharp leading edges. A chine with wedge cross-section was added to the forebody 0.5 in. above the wing. See Fig. 1 for the planform view, side view, and two cross-sectional views of the model. The model was equipped with a total of 80 upper-surface static pressure taps loaded at 30, 40, 50, 62.5, and 75% of the distance along the wing centerline chord as depicted in Fig. 1. The wing was mounted on a generic fuselage that accommodated a four-module Scanivalve and a six-component balance.

The model was tested in the David Taylor Naval Ship Research and Development Center's 7- × 10-ft transonic tunnel

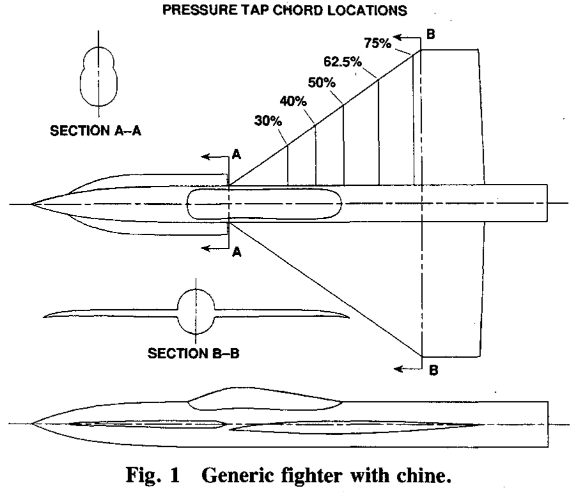

Fig. 1 Generic fighter with chine.

Presented as Paper 90-6.4.2 at the 17th Congress of the International Council of the Aeronautical Sciences, Stockholm, Sweden, Sept. 9–14, 1990; received Jan. 26, 1991; revision received Aug. 8, 1991; accepted for publication Aug. 12, 1991.

*Aerospace Engineer, Advanced Aerodynamic Concepts Branch, Aerodynamics Division. Member AIAA.

at Mach numbers between 0.40 and 0.95 and at angles of attack between 0 and 22 deg. The effects of Mach number, angle of attack, and the leading-edge flap deflection on the wing upper-surface static pressure distributions were studied.[2] The model was also tested in the NASA Ames Research Center's 6- × 6-ft wind tunnel at Mach numbers between 0.40 and 1.8, and at angles of attack between 0 and 24 deg. The emphasis in the Ames test was to determine the changes in the flowfield over the wing made by placing a chine at various locations on the forebody.[5]

Computational Work

Computational fluid dynamics (CFD) is becoming increasingly important in the analysis and understanding of flows about complex configurations. Wind-tunnel data is often limited by instrumentation constraints, flow quality, wall and support interferences, and aeroelastic effects. In contrast, CFD codes provide detailed information about the entire flowfield, thus they are helpful in understanding off-body flowfield characteristics. The validation of CFD codes for a wide range of flight conditions is essential if they are to become useful tools in aerodynamic design and analysis. With the advent of supercomputers such as the Cray-2 and the Cray Y-MP, it is now possible to compute Euler and Navier-Stokes solutions for complex geometries using denser grids, thus improving upon the accuracy of the solutions obtained in the past. The numerical solutions of the Euler and Navier-Stokes equations are not yet at the production level at which they can be easily applied to any configuration and flight condition. The generation of a suitable grid about a complex configuration remains one of the most challenging problems in the field of CFD.

Euler Solution Procedure

The Euler equations govern the adiabatic flow of an inviscid, ideal gas. The application of Euler methods to the prediction of vortical flow about delta wings and slender bodies at angle of attack remains the source of considerable controversy. How separation occurs in the numerical simulation of an inviscid flow, and the degree of realism that the inviscid model provides in describing the actual flow physics, have not yet been thoroughly established. Following Newsome,[1] Crocco's theorem is applied to show that theoretically valid solutions to the Euler equations with flow separation do exist. However, the solutions do not necessarily provide an accurate description of the separation that occurs in the actual viscous flow.[6] Numerical solutions of separated flows can be explained by the addition of dissipation in the computational algorithm required for stability. Several studies have been performed to examine the effect of dissipation on the solutions of flows about delta wings. Powell et al.[7] have argued that a Kutta condition exists at a sharp leading edge that fixes the point of separation at the leading edge independent of the amount of dissipation added. The only requirement is that the computational model have a diffusive effect at the leading edge that mimics physical viscous diffusion. Because of truncation error and added artificial viscosity, the discretized Euler equations are diffusive near the leading edge.

The numerical algorithm FLO57 was originally written by Jameson[8] and was modified by Melton to accommodate an O–H grid topology. The method is a finite-volume multistage technique which is second-order accurate on a smooth grid. Since the numerical algorithm is not inherently dissipative, artificial viscosity must be added to the discretized equations to provide stability. The added dissipation includes second- and fourth-difference terms. The fourth-difference term is third order and provides dissipation in smooth regions. The second-difference term is proportional to the second difference in pressure and is first order. This term limits shock oscillations, thereby allowing shock capturing, and is significant in regions of rapid expansion. The tangential flow boundary condition is enforced on the solid body whereas the Kutta condition at the sharp leading and trailing edges is held implicitly in the numerical integration.[9]

The grid generated about the generic fighter has an O–H topology which allows good leading-edge resolution compared to other topologies. The grid was generated using an elliptic solver which was written by Melton. This code solves the Laplace equation in two dimensions in order to smoothly wrap a grid around the body at specific longitudinal locations. This grid is then algebraically redistributed in the direction normal to the wing surface to provide a user-specified clustering near the wing surface and also to provide a smooth transition between grid planes in the streamwise direction.

The grid used in all of the computations has 426,790 grid points: 134 points in the streamwise direction with 74 points on the body, 49 points from the wing surface to the outer boundary, and 65 points circumferentially around the body. The grid extends 6.5 centerline chord lengths upstream and downstream of the body and 7 semispan lengths radially to the outer boundary. The chine was modeled as a flat plate. The surface grid for the wing/body model and two crossflow planes are illustrated in Ref. 10.

Results and Discussion

FLO57 solutions were obtained at Mach numbers of 0.8 and 1.2 for the wing/body configuration and 0.8, 1.2, and 1.6 for the wing/body/chine configuration. A minimum of 1200 iterations at the low angles of attack and 3000 to 3500 iterations at the higher angles were necessary to ensure that the residuals decreased at least three orders of magnitude. The lift, drag, and moment histories show convergence after about 1000 iterations while the residuals are still decreasing. All solutions were obtained on either the Cray-2 or the Cray Y-MP at NASA Ames Research Center. The memory requirement was approximately 12 MW, and the CPU time required for 1000 iterations was approximately 10,300 s on the Cray-2 and approximately 4800 s on the Cray Y-MP. Thus, each solution took 4 to 10 h to obtain on the Cray-2 and 2 to 4 h on the Cray Y-MP. Computed pressure coefficients at the 30, 40, 50, 62.5, and 75% chord stations along with lift, drag, and pitching moment for each Mach-alpha combination were compared to the experimental results. A discussion of the results for each combination of Mach number and configuration will be presented in the following sections.

Mach 0.8 Wing/Body

The FLO57 pressure distributions compare well over the entire wing with experimental results at $\alpha = 5$ deg, where the flow is attached and there is no leading-edge vortex. The shape of the pressure distribution is accurately modeled. The experimental results show that a vortex has begun to form close to the leading edge at $\alpha = 8$ deg. The numerical results do not correlate as well with experimental results as they do at the lower angle of attack. The Euler results show the formation of a weaker vortex that lies inboard of the experimental vortex. Since the vortex is just starting to form, the Euler solution may be sensitive to the grid density and the numerical definition of the leading-edge geometry. See Ref. 10 for the pressure distributions at $\alpha = 5$ deg and at $\alpha = 8$ deg.

The pressure distributions at $\alpha = 12$ deg are given in Figs. 2a–d. The Euler solution does not predict the strength of the vortex core accurately at this condition. The numerical pressure distribution tends to flatten toward the trailing edge of the wing which appears to indicate vortex breakdown. Further evidence of vortex breakdown is given by numerical simulations of particle paths which show recirculation within the vortex core.

The Euler solutions show poor agreement with experimental results at both $\alpha = 16$ deg and $\alpha = 20$ deg. The FLO57 results do not show a distinct vortex at either angle, but instead have flat spanwise pressure distributions, as shown in Ref. 10. In addition, the moment histories in Ref. 10 are

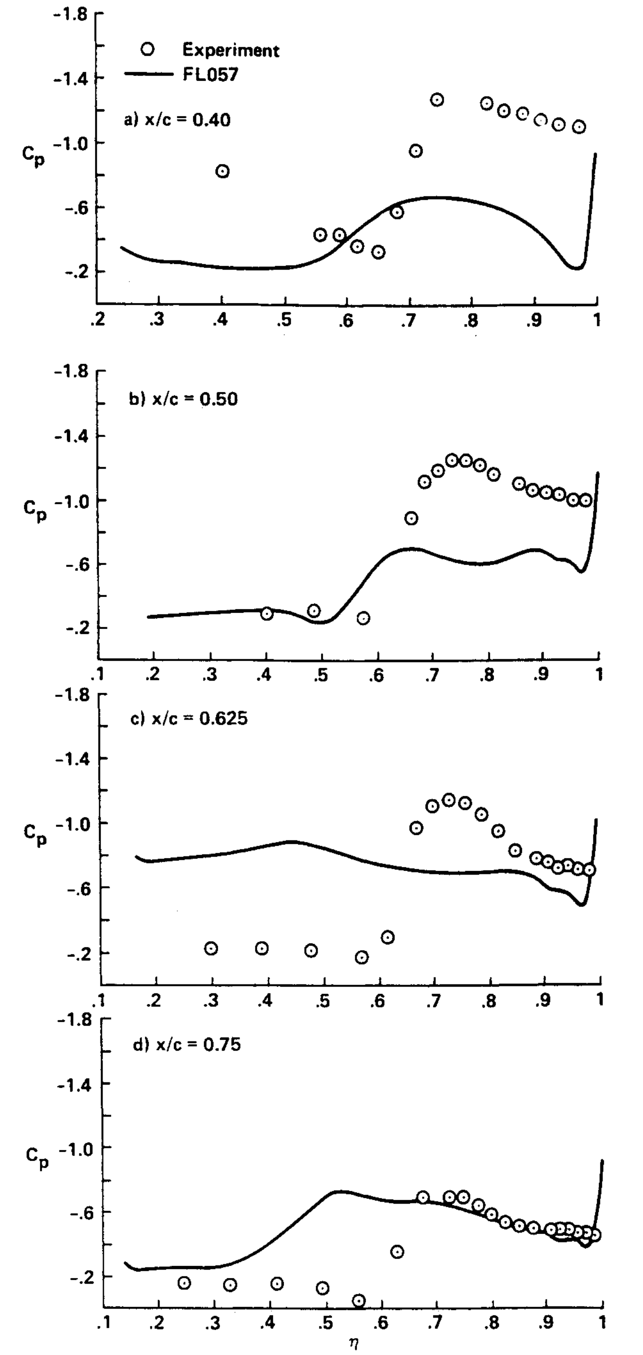

Fig. 2 Upper surface pressure distributions for wing/body, M_∞ = 0.8 and α = 12.0 deg.

unstable and oscillatory for both angles with a large increase in nose-down pitching moment. These flat distributions and random moment histories may be an indication of vortex breakdown. The experimental results show a flattening of the pressure distributions aft of the 50% chord station. Oil flow photos also show an abrupt expansion of the vortex which may be an indication of vortex breakdown.[5] The lift, drag, and moment coefficient curves show good agreement until about α = 12 deg (Figs. 3a–c). As the appearance of vortex breakdown becomes more extensive, the Euler predictions lose their accuracy.

Mach 0.8 Wing/Body/Chine

The overall agreement between computational and experimental results improved with the addition of the chine. Without the chine, the flow over the forebody is strongly affected by viscous separations. These effects cannot be modeled in

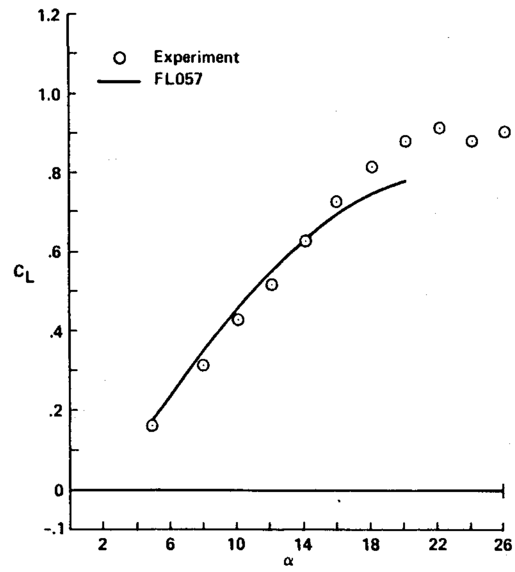

a) Lift curve

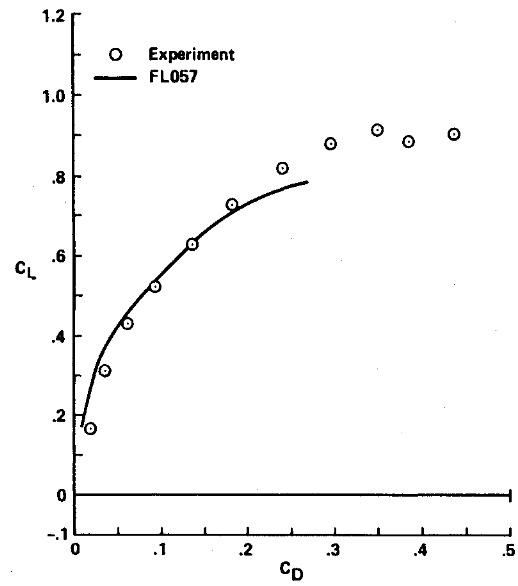

b) Drag polar

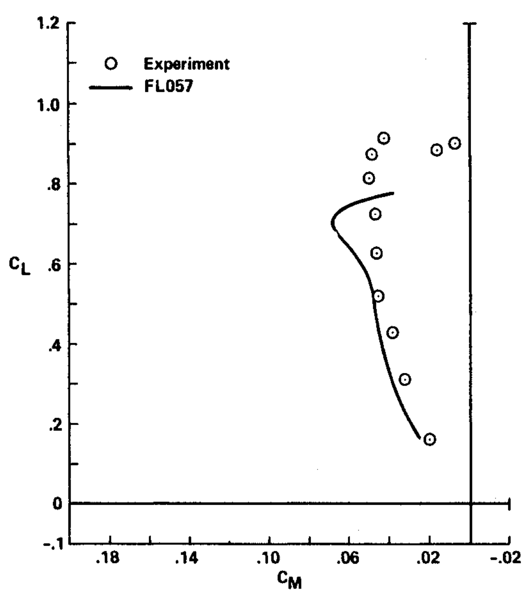

c) Moment curve

Fig. 3 Experiment-CFD forces and moments for wing/body, M_∞ = 0.8.

an Euler simulation. The dominant vortex from the chine is captured by the Euler code, allowing FLO57 to provide a more representative model of the forebody flowfield as it approaches the apex of the main wing.

At α = 8 deg, the Euler code has difficulty modeling the start of the vortex as previously described, and the correlation is not as good. The pressure distributions at α = 12 deg are given in Figs. 4a–d. The Euler results accurately predict the location and strength of the vortex over most of the wing and do not indicate breakdown as seen with the wing/body configuration. Also, the moment history is smoother than that from the wing/body case.

Both Euler and experimental results at α = 16 deg and α = 20 deg show that placing the chine on the forebody delays the onset of instabilities that lead to vortex breakdown. This is clearly evident by comparing the moment histories from the wing/body/chine configuration with those from the wing/body configuration.[10] The plots in Ref. 10 indicate that the

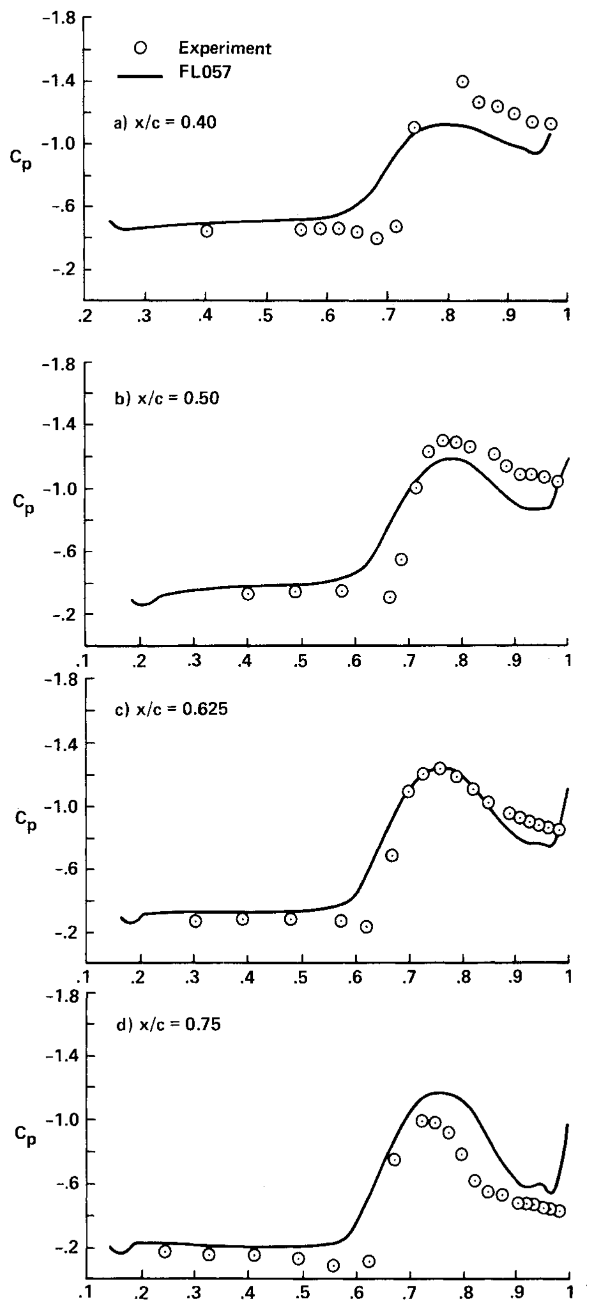

Fig. 4 Upper surface pressure distributions for wing/body/chine, M_∞ = 0.8 and α = 12.0 deg.

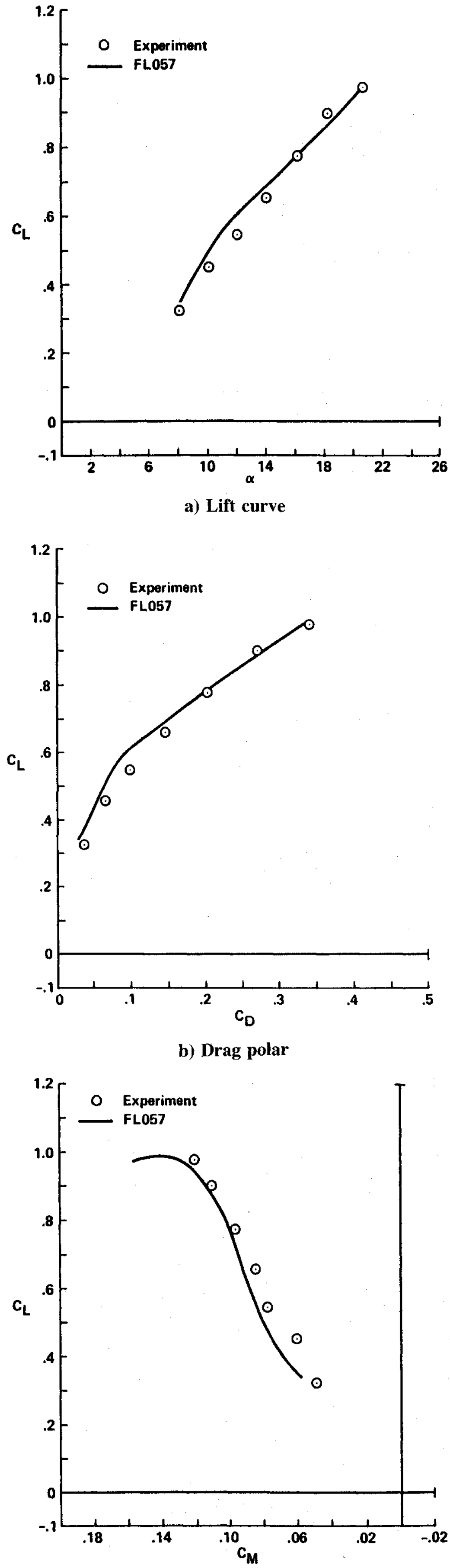

a) Lift curve

b) Drag polar

c) Moment curve

Fig. 5 Experiment-CFD forces and moments for wing/body/chine, M_∞ = 0.8.

moment coefficients were still oscillatory but were less random. The increase in lift and the decrease in drag from the wing/body results are overpredicted by FLO57 (Figs. 5a and 5b). The shape of the moment curve was accurately predicted by the Euler code, as shown in Fig. 5c.

Mach 1.2 Wing/Body

In general, the pressure correlation between the Euler and experimental results improved in supersonic flow at all angles of attack. At $\alpha = 4$ deg, the shape of the pressure distribution is accurately predicted. At $\alpha = 8$ deg, the computational results show good correlation with the experimental pressures inboard of approximately 90% of the local semispan at all chordwise stations. Outboard of this location, the experimental results show a suction peak that is larger than that shown computationally. This may be attributed to poor grid resolution at the leading edge. The supersonic pressure dis-

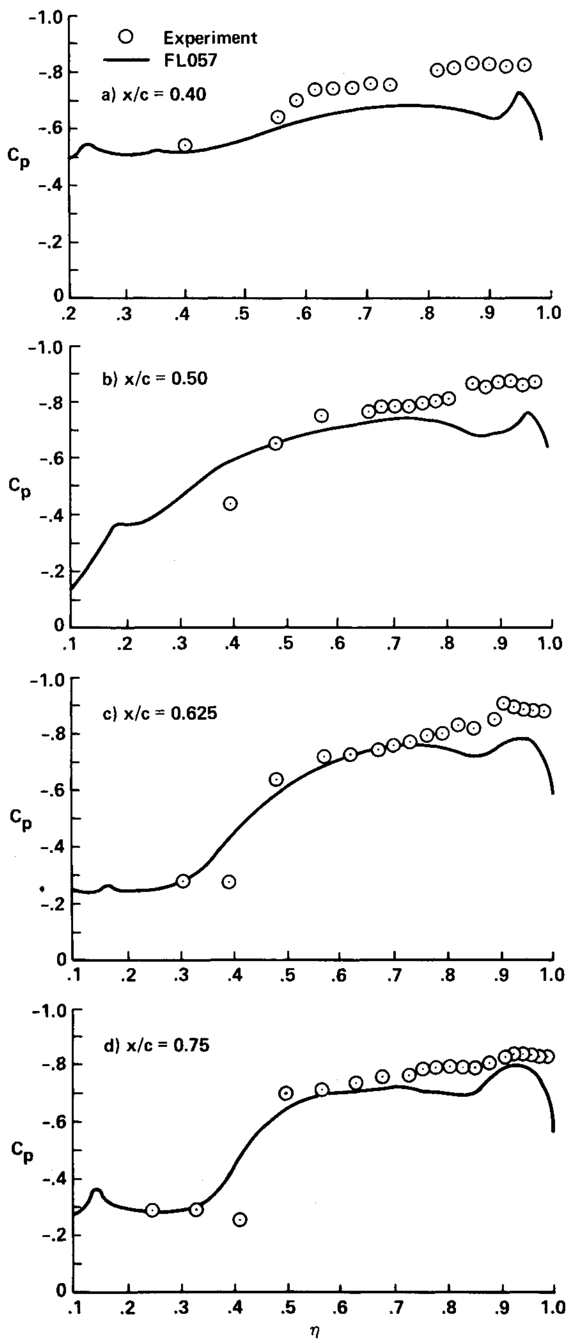

Fig. 6 Upper surface pressure distributions for wing/body/chine, $M_\infty = 1.2$ and $\alpha = 16.0$ deg.

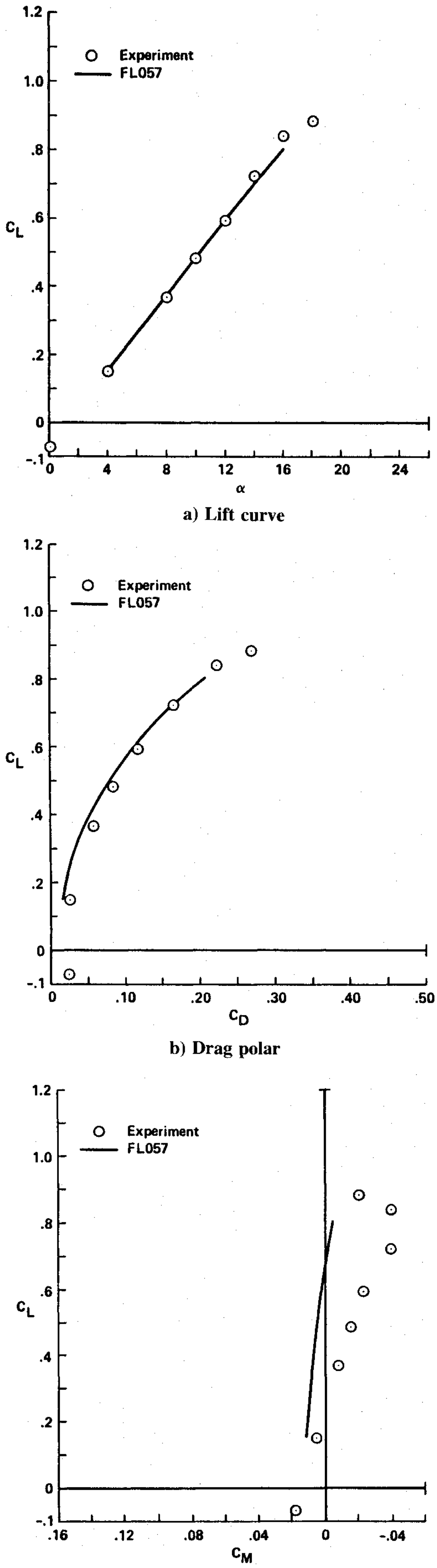

Fig. 7 Experiment-CFD forces and moments for wing/body/chine, $M_\infty = 1.2$.

tributions not shown in this report appear in NASA Technical Publication 3156, November 1991).

The computational results are accurate inboard of approximately 80% of the local semispan at $\alpha = 12$ deg. The experimental data show a greater suction peak near the leading edge and a greater surface area over which the lower pressures exist. The computational velocity vectors show that a leading-edge vortex forms at about 50% of the chord. The vortex is flat and close to the surface. The fact that the vortex does not form until this point suggests that the grid density may not be sufficient to capture a weak vortex upstream of this location.

The computational results do not correlate as well with experimental pressure coefficients at $\alpha = 16$ deg. However, the correlation tends to improve with increasing streamwise location, as shown in Figs. 6a–d. The computational velocity vectors show that a leading-edge vortex does form at the apex

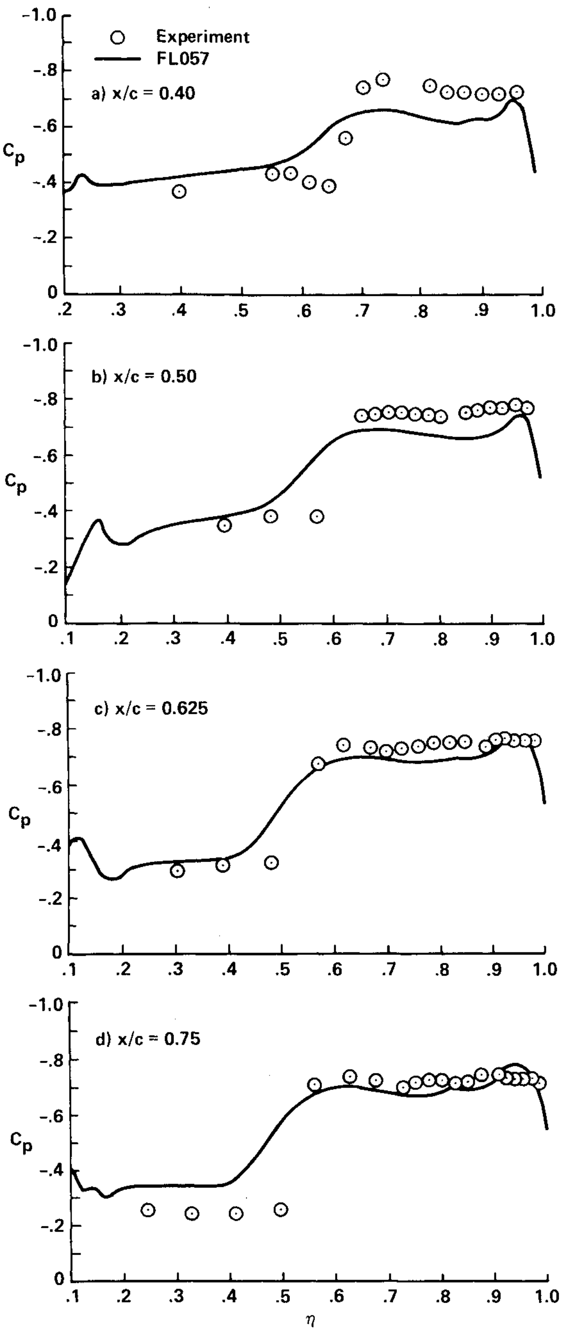

Fig. 8 Upper surface pressure distributions for wing/body/chine, $M_\infty = 1.2$ and $\alpha = 16.0$ deg.

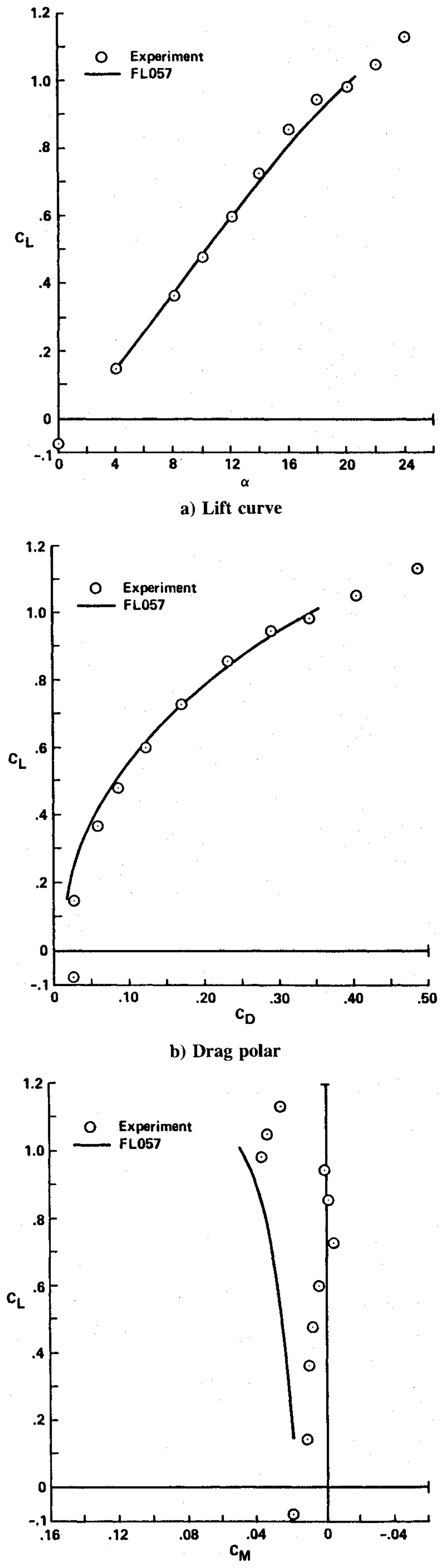

a) Lift curve

b) Drag polar

c) Moment curve

Fig. 9 Experiment-CFD forces and moments for wing/body/chine, $M_\infty = 1.2$

of the wing. Also, the velocity vectors show that at supersonic Mach numbers the location of the vortex core is more inboard, and the vortex flattens and lies closer to the surface, than at subsonic Mach numbers. This is also seen experimentally, as described by Erickson in Ref. 5.

The lift, drag, and moment comparisons are given in Figs. 7a–c. The lift comparison is good through $\alpha = 12$ deg.

Mach 1.2 Wing/Body/Chine

The addition of the chine at supersonic speeds does not cause a marked improvement in the correlation between the pressures and forces that was seen at the subsonic Mach numbers. The pressure distribution is nearly identical for the wing/body and wing/body/chine configurations at $\alpha = 4$ deg. At $\alpha = 8$ deg and $\alpha = 12$ deg, the trends are similar between the two configurations, but the chine tends to increase the pressures on the upper surface. The addition of the chine brings the experimental and computational results into closer agreement at $\alpha = 16$ deg (Figs. 8a–d). At $\alpha = 20$ deg, the com-

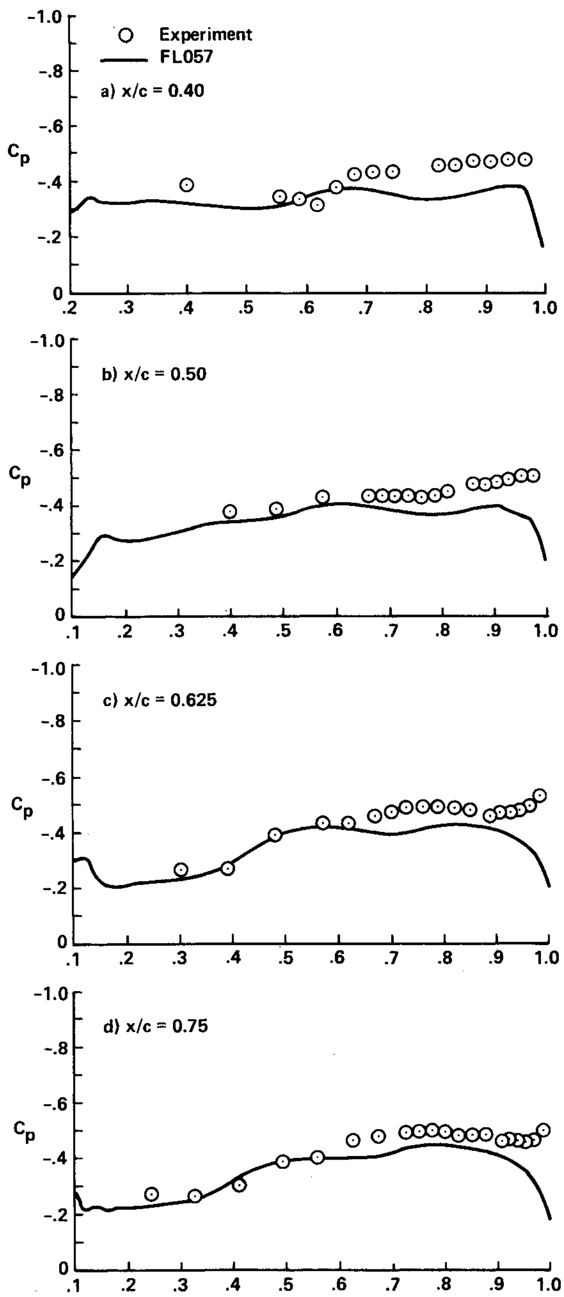

Fig. 10 Upper surface pressure distributions for wing/body/chine, $M_\infty = 1.6$ and $\alpha = 16.0$ deg.

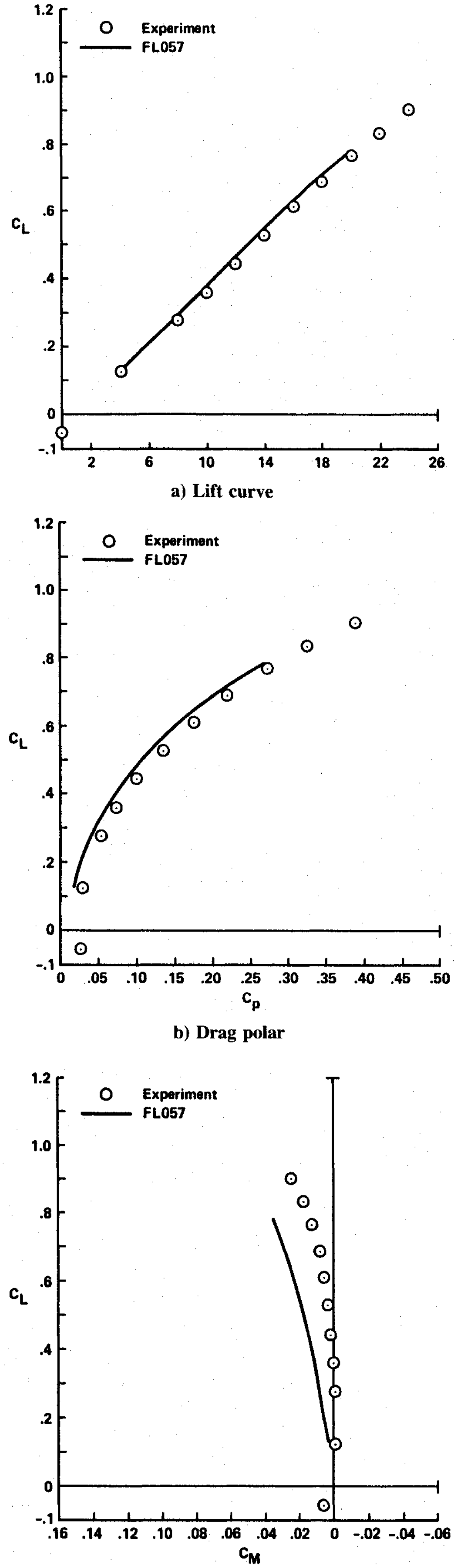

a) Lift curve

b) Drag polar

c) Moment curve

Fig. 11 Experiment-CFD forces and moments for wing/body/chine, $M_\infty = 1.6$.

parison between the pressure distributions is not as good inboard of approximately 60% of the local semispan but does improve outboard of that location. The inboard pressures computed by FLO57 are higher than the experimental pressures. The oil flow at this condition shows the existence of a cross-flow shock located between the vortex and wing upper surface which induces secondary separation as described in Ref. 5. Along the shock, there is an abrupt change in the direction of the flow on the surface. By analyzing the pressure distribution, it can be seen that the shock is not a strong one since the pressure rise is slight. This shock is not captured in the Euler solution. Secondary separation is also observed in the oil flow. In addition, the oil flow shows a small recirculation region between the location of the crossflow shock and the tip near the trailing edge of the wing which is not captured in the Euler simulation.

Force and moment coefficient comparisons are presented in Figs. 9a–c. The lift and drag show good agreement through $\alpha = 12$ deg.

Mach 1.6 Wing/Body/Chine

The shapes of the pressure distributions are accurately predicted by FLO57 at $\alpha = 4$ deg. At $\alpha = 8$ deg, the suction peak shown at the lower supersonic Mach numbers has diminished even further and has disappeared aft of the 50% chord station. The correlation between FLO57 and experiment is good at the last two chord stations. The Euler results show attached flow at angles less than $\alpha = 12$ deg. At $\alpha = 12$ deg, the correlation between pressures is good downstream of the 50% chord location. At the stations closer to the apex, the Euler pressures are higher than those seen in the experimental data outboard of approximately 80% of the local semispan. Inboard of this position the pressures are accurately predicted by FLO57. The correlation between pressure distributions is not as good as that at $M_\infty = 1.2$, with FLO57 predicting higher pressures than experiment at $\alpha = 16$ deg (Figs. 10a–d).

The slope of the lift curve computed by the Euler code is slightly higher than given in the experimental results (Fig. 11a). Also, the drag data contain a greater offset than before (Fig. 11b). The displacement of the moment curve has decreased, although the slope predicted by FLO57 is still too large (Fig. 11c).

Conclusion

The FLO57 Euler code has been used to calculate transonic and supersonic flow solutions over two configurations of a generic fighter model. Results were computed at Mach numbers 0.8, 1.2, and 1.6 for angles of attack between 4 and 20 deg.

Although the Euler code predicts attached flow well, it is less accurate when the leading-edge vortex is just beginning to form. This may be due to the sensitivity of FLO57 to grid resolution and geometric modeling of the leading edge. For the transonic case, the Euler results are in good agreement with experiment until vortex breakdown occurs in the solutions. The results presented in this paper show that the Euler code tends to predict breakdown prematurely. When the experimental results indicate vortex breakdown, the agreement between pressure distributions improves. For the supersonic cases, vortex breakdown was not observed in the Euler solutions. Overall, the supersonic results were in better agreement with wind-tunnel data than the transonic case was.

The effect of adding the chine on the forebody was most noticeable in transonic flow, where its addition delayed the onset of vortex breakdown both numerically and experimentally and improved the Euler predictions of the pressure distributions. The decoupled chine vortex interacts favorably with the wing flowfield, and acts to increase the effective leading-edge sweep.[5] The FLO57 comparisons improve with the addition of the chine because the chine fixes the forebody separation location along its leading edge and provides a dominant flow feature which the Euler code can capture. Without the chine, the Euler code cannot model the flow approaching the main wing correctly, especially at high angles of attack, because the character of the incoming flowfield is largely dependent upon forebody boundary-layer separations. In supersonic flow the favorable effect of the chine is not seen, because the solutions do not show vortex breakdown at any of the angles of attack obtained with the Euler code. The main effect of the chine in supersonic flow is to push the leading-edge vortex outboard.

References

[1]Newsome, R. W., and Kandil, O. A., "Vortical Flow Aerodynamics—Physical Aspects and Numerical Simulation," AIAA Paper 87-0205, Reno, NV, Jan. 1987.

[2]Erickson, G. E., and Rogers, L. W., "Experimental Study of the Vortex Flow Behavior on a Generic Fighter Wing at Subsonic and Transonic Speeds," AIAA Paper 87-1262, Honolulu, HI, June 1987.

[3]Stanbrook, A., and Squire, L. C., "Possible Types of Flow at Swept Leading Edges," *Aeronautical Quarterly*, Vol. XV, Pt. 1, Feb. 1964, pp. 72–82.

[4]Miller, D. S., and Wood, R. M., "Lee-Side Flow Over Delta Wings at Supersonic Speeds," NASA TP 2430, June 1985.

[5]Erickson, G. E., Rogers, L. W., Schreiner, J. A., and Lee, D. G., "Subsonic and Transonic Vortex Aerodynamics of a Generic Forebody Strake-Cropped Delta Wing Fighter," AIAA Paper 88-2596, Williamsburg, VA, June 1988.

[6]Fujii, K., and Schiff, L. B., "Numerical Simulation of Vortical Flows Over a Strake-Delta Wing," AIAA Paper 87-1229, Honolulu, HI, June 1987.

[7]Powell, K. G., Murman, E. M., Perez, E., and Baron, J., "Total Pressure Loss in Vortical Solutions of the Conical Euler Equations," AIAA Paper 85-1701, Cincinnati, OH, July 1985.

[8]Jameson, A., and Baker, T. J., "Solution of the Euler Equations for Complex Configurations," AIAA Paper 83-1929CP, *AIAA 6th Computational Fluid Dynamics Conference*, AIAA, New York, July 1983.

[9]Powell, K. G., "Vortical Solutions of the conical Euler Equations," Ph.D. thesis, Massachusetts Inst. of Technology, Boston, MA, 1987.

[10]Goodsell, A. M., Madson, M. D., and Melton, J. E., "TranAir and Euler Computations of a Generic Fighter Including Comparisons with Experimental Data," AIAA Paper 89-0263, Reno, NV, Jan. 1989.